



# **Scoliosis Detection: Edge-Preserving Preprocessing of Spinal X-Rays Using PDEs and Deep Learning-Based Classification**

**Systems & Biomedical Engineering Department  
Special Functions & Partial Differential Equations  
(MTH2245)  
Chasing Arcs**

# ARC'S TEAM

N ame	B.N.	ID
Ekram Ahmad Auf Mohamed	12	9230228
Raghad Abdelhameed Abdelhady Abdelhameed	28	9230371
Zeyad Ashraf Ahmed Mohamed	30	9230391
Salma Ali Ibrahim Ali	35	9230439
Abdlrhman Reda Khalaf Mohamed	42	9220428

# Table of Contents

<b>1. Abstract</b>	<b><a href="#">5</a></b>
<b>2. Introduction</b>	<b><a href="#">6</a></b>
<b>3. Problem Definition</b>	<b><a href="#">8</a></b>
3.1 Problem	<a href="#">8</a>
3.2 Objective	<a href="#">8</a>
3.3 Mathematical Formulation	<a href="#">8</a>
3.3.1 Pre-processing Stage	<a href="#">8</a>
3.3.2 Classification Stage	<a href="#">8</a>
3.3.3 Regression Stage	<a href="#">9</a>
<b>4. Dataset</b>	<b><a href="#">10</a></b>
<b>5. Methodology</b>	<b><a href="#">11</a></b>
5.1 Heat Equation	<a href="#">11</a>
5.2 Anisotropic Diffusion	<a href="#">13</a>
5.3 Classification Stage using CNN	<a href="#">14</a>
5.3.1 Model Architecture	<a href="#">15</a>
<b>6. Experimental Work</b>	<b><a href="#">18</a></b>
6.1 Introduction to Experimental Setup	<a href="#">18</a>
6.2 Data Description	<a href="#">18</a>
6.3 Model Architecture	<a href="#">19</a>
6.4 Training Methodology	<a href="#">20</a>
6.5 Image Preprocessing for Cobb Angle Calculation	<a href="#">21</a>
<b>7. Results</b>	<b><a href="#">22</a></b>
7.1 Comparison of Heat Equation and Anisotropic Diffusion for Pre-processing Spinal X-ray Images	<a href="#">22</a>
7.2 Structural Similarity Index Measurements (SSIM)	<a href="#">24</a>
7.3 Summary Results of the CNN model's performance	<a href="#">25</a>
7.4 Summary Results of the CNN model's performance	<a href="#">26</a>
<b>8. Conclusion</b>	<b><a href="#">27</a></b>
<b>9. References</b>	<b><a href="#">28</a></b>

# List of Abbreviations

• AIS	Adolescent Idiopathic Scoliosis
• PDEs	Partial Differential Equations
• CNN	Convolutional Neural Network
• 3D	Three-Dimensional
• HDE	Heat Diffusion Equation
• PM	Perona and Malik
• PhD	Doctor of Philosophy
• PT	Physical Therapist
• MSc	Master of Science
• API	Application Programming Interface
• ReLU	Rectified Linear Unit
• 1D	One-Dimensional
• SSIM	Structural Similarity Index Measurements

# 1. Abstract

Scoliosis is an abnormal curvature of the human spinal column, often accompanied by vertebral rotation. Adolescent Idiopathic Scoliosis (AIS) is the most common type, typically affecting children between 8 and 18 years old during bone growth at its maximum rate. Early detection of scoliosis often allows for non-surgical treatment options, such as physiotherapy and using specific braces like the Boston Brace or Milwaukee Brace. This research proposes an innovative approach to enhance the accuracy of spinal X-ray image analysis. We aim to improve image quality and diagnostic accuracy by combining the power of Partial Differential Equations (PDEs), specifically the Heat Equation and Anisotropic Diffusion, for pre-processing and a Convolutional Neural Network (CNN) for classification. The pre-processing stage reduces noise and preserves fine details, while CNN classifies images as normal or indicative of scoliosis. We expect significant improvements in noise reduction, and edge preservation, leading to higher classification accuracy and aiding in early diagnosis and efficient treatment planning for scoliosis.

## 2. Introduction

Scoliosis, a 3D deformation of the human spinal column, is characterized by a lateral curvature of the spine and axial rotation of the vertebrae. Adolescent Idiopathic Scoliosis (AIS) is the most common type, comprising about 80% of pediatric scoliosis and affecting about 3% of adolescents under the age of 16. Scoliosis treatment is highly dependent on the shape and degree of spinal curvature, and while guidelines have been established for best management practices, individual treatment options are based on surgeon experience. Therefore, the development of a clinically validated, patient-specific model of the spine to aid surgeons in understanding AIS in its early stages and inform optimal surgical and non-surgical treatment could provide substantial clinical value [1].

Medical imaging systems are important in doctors' diagnosis processes [2,3]. Using medical images, doctors have information about the internal parts of the body and the organs [4]. Doctors can diagnose complex diseases much more accurately Through medical images that are different from other image types in terms of the information obtained by pixels [5]. Different types of imaging techniques are used for the different parts of the human body [6].

X-ray imaging is a technique that is mostly used in the regions between the bones and the tissue around the bones [7]. X-rays are a valuable diagnostic tool that uses electromagnetic radiation to create images of the inside of the body, aiding in the detection of various medical conditions such as fractures, tumors, and infections. They are non-invasive, relatively quick, and widely available, making them an essential part of modern healthcare. However, one of the disadvantages of X-ray technology is the potential for noise in the images, which can sometimes obscure details and make diagnosis more difficult [8]. Noise in medical X-ray images is primarily categorized into quantum mottle, which is related to the number of incident X-rays, and artificial noise is due to the grid, etc., [9]. Noise is usually generated in the process of acquisition and transmission of images; this affects the visual quality of an image.

Denoising the image without affecting the edge information is a challenging problem in image processing [10-14]. Denoising is usually used as a pre-processing step in many image applications such as medical applications, image segmentation, edge detection, image enhancement, and image decomposition. Filter-based methods such as Median filter, and Gaussian filter [15,16] are commonly used for this purpose, as these are simple and easy to implement. The main drawback of these filters is, these filters annihilate important details and blur prominent geometrical edges because a fixed filter is applied to all pixels of the image, whether these pixels are noisy or not. Therefore, the median and Gaussian filters are not appropriate choices for many image-smoothing applications [17-19].

Techniques based on partial differential equations (PDEs) are widely used in image denoising [20]. According to [21] In 1984, the heat diffusion equation (HDE) in image processing to obtain a parametric family generated by an image. HDE is an isotropic heat diffusion equation with uniform diffusion of the image in all directions that causes the edges to blur during smoothing [22].

Results obtained from isotropic diffusion are similar to the results obtained from Gaussian convolution of the image [23, 24]. To overcome this drawback of isotropic HDE, Perona and Malik (PM) proposed anisotropic diffusion [25]. Perona and Malik, for the first time, used Anisotropic diffusion for image smoothing without affecting the edge information much by decreasing diffusivity near edge locations [27]. In the PM method, the diffusion coefficient function is taken as a decreasing function of the gradient magnitude of the image varying with space and time [28-30].

Various techniques via anisotropic diffusion have been developed to remove noise and edge preservation [31] simultaneously. These techniques are based on gradient vector flow [32-35]. A fast and flexible denoising convolutional neural network (CNN) has been applied for image denoising [36]. This method works on the down-sampled sub-images to give effective results. This convolutional neural network (CNN) based technique performs better for synthetic noisy images [37,38]; however, their performance is limited to real noisy images [39-42]. The CNN model was trained on a dataset of spine X-ray images, with each image labeled as either "scoliosis" or "normal." The model successfully learned to identify key features associated with scoliosis, such as spinal curvature and vertebral rotation, enabling accurate classification of new, unseen X-ray images. This automated approach has the potential to significantly improve the efficiency and accuracy of scoliosis diagnosis, leading to earlier intervention and better patient outcomes [43-46].

The main objective behind all the above-mentioned approaches is the application of the heat equation and anisotropic diffusion for pre-processing X-ray images. The proposed approach involves a two-step process: initial noise reduction using the heat equation, followed by edge-preserving smoothing using anisotropic diffusion, leading to improved diagnostic accuracy. followed by a Convolutional Neural Network (CNN) for classification. The primary objective is to develop a robust and efficient method for scoliosis detection that overcomes the limitations of existing approaches and achieves superior performance.

## 3. Problem Definition

### 3.1. Problem:

Scoliosis, a lateral curvature of the spine, is a common condition that can lead to significant health issues if left untreated. Early detection is crucial for effective treatment. However, accurate diagnosis from spinal X-rays can be challenging due to noise and image degradation, which can hinder the performance of automated classification algorithms.

### 3.2. Objective:

The goal is to improve the accuracy of a Convolutional Neural Network (CNN) model for classifying spinal structures while ensuring that the model retains crucial information about the spinal anatomy.

### 3.3. Mathematical Formulation:

#### 3.3.1. Pre-processing Stage:

##### 1. Heat Equation:

$$\frac{\partial u}{\partial t} = \alpha \nabla^2 u \quad [48]$$

Where:

- $u(x,y)$  is image intensity at position  $(x, y)$  and time  $t$ .
- $\frac{\partial u}{\partial t}$  is the time derivative of the image intensity.
- $\alpha$  is diffusion coefficient, controlling the rate of diffusion.
- $\nabla^2$  is the Laplacian operator, measuring the curvature of the image intensity.

Apply the heat equation to reduce noise in the image by diffusing the image intensity over time, thereby smoothing out noise.

##### 2. Anisotropic Diffusion:

$$\frac{\partial I_t(x,y)}{\partial t} = \nabla \cdot (c(|\nabla I_t|) \nabla I_t) \quad [30]$$

Where:

- $I_t(x, y)$  is the image intensity at position  $(x, y)$  and time  $t$ .
- $\nabla$  is the gradient operator.
- $c(|\nabla I_t|)$  is a diffusion coefficient that depends on the gradient magnitude.

Apply anisotropic diffusion to preserve edges while reducing noise, with the diffusion coefficient  $c(|\nabla I|)$  functioning as a gradient magnitude-based factor for selective smoothing.



### **3.3.2. Classification Stage:**

#### **1. Convolutional Neural Network (CNN):**

- o Train a CNN model on a large dataset of labeled spinal X-ray images.
- o CNN extracts relevant features from the pre-processed images and classifies them as normal or scoliotic. [\[39-42\]](#)

### **3.3.3. Regression Stage:**

#### **1. Landmark Detection:**

- o A regression model is used to identify key vertebral landmarks on the spinal X-ray, such as the upper and lower endplates of the most tilted vertebrae.

#### **2. Angle Calculation:**

- o Apply a regression algorithm to compute the tilt angles of the identified vertebrae.

#### **3. Cobb Angle Measurement:**

- o Use the predicted tilt angles to calculate the Cobb angle, quantifying the severity of scoliosis. [\[43-46\]](#)

By combining these techniques, the goal is to enhance the quality of spinal X-ray images, making them more suitable for accurate automated classification and, ultimately, improving the early detection and management of scoliosis.

## 4. Dataset

This research aims to detect scoliosis early, as early diagnosis can prevent the need for surgery. In the early stages, treatment primarily involves bracing and physiotherapy. Common types of braces used are:

- **Boston Brace:** This is a rigid brace that applies pressure to correct spinal curvature.
- **Milwaukee Brace:** This brace extends from the chin to the pelvis and is used for more severe curvatures.



*Boston Brace*



*Milwaukee Brace*

To achieve this objective, we collected a comprehensive dataset of spinal X-ray scans from various sources, with a specific focus on **Egyptian patient data**. Our data sources include:

- **Clinics specializing in scoliosis treatment:**
  - o ARC for Scoliosis Physiotherapy (Dr. Mahmoud Ibrahim, PhD, PT)
  - o ScolioCare ( Dr. Sarah M.Ali, MSc, PT)
  - o الفقري العمود لتأهيل قوام (Dr. Tayseer Saber Abdeldayem)
  - o 4kids Therapy Clinic ( Dr. Sarah M.Ali, MSc, PT)
- **Open-source datasets:**
  - o <https://data.mendeley.com/datasets/xkt857dsxk/1> (A dataset of scoliosis, spondylolisthesis, and normal vertebrae X-ray images)
  - o <https://universe.roboflow.com/scoliosis/scoliosis-myka6/dataset/1> (Scoliosis dataset from Roboflow universe)

This diverse dataset, comprising over 580 normal scans and over 765 scoliosis scans, will allow us to train a robust and generalizable model for accurate scoliosis detection in X-ray images.

## 5. Methodology

### 5.1. Heat Equation: A Smoothing Technique for Noise Reduction

The heat equation, a partial differential equation, is employed in image processing to model intensity diffusion, where pixel values are treated like temperatures. This diffusion process causes high-intensity (brighter) areas to spread toward lower-intensity (darker) areas, creating a smoothing effect that reduces sharp edges and noise. Applied to medical images, this technique enhances subtle features critical for scoliosis detection. By adjusting parameters, the method optimizes clarity and sensitivity, facilitating early detection by refining image details and minimizing noise.

**Mathematically, the heat equation is expressed as:**

$$\frac{\partial u}{\partial t} = \alpha \nabla^2 u \quad [48]$$

Where:

- $u(x,y)$  is image intensity at position  $(x, y)$  and time  $t$ .
- $\frac{\partial u}{\partial t}$  is the time derivative of the image intensity.
- $\alpha$  is diffusion coefficient, controlling the rate of diffusion.
- $\nabla^2$  is the Laplacian operator, measuring the curvature of the image intensity.

#### Implementation Steps:

1. **Discrete Approximation of the Laplacian:** In a discrete grid (image matrix), the Laplacian at pixel  $(i, j)$  can be approximated by the second difference:

$$\nabla^2 u(i, j) \approx u(i+1, j) + u(i-1, j) + u(i, j+1) + u(i, j-1) - 4u(i, j)$$

This approximation sums the values of the neighboring pixels, subtracting four times the center pixel's value, capturing the “smoothness” at that point.

2. **Finite Difference Scheme for Time Evolution:** To solve the heat equation numerically, we use a finite difference scheme in time as well. Discretizing in time with a small timestep  $dt$ , we update the pixel value  $u(i, j)$  at each step:

$$u(i, j)^{\text{new}} = u(i, j)^{\text{old}} + \alpha \cdot dt \cdot \nabla^2 u(i, j)$$

In each iteration, this equation updates  $u(i, j)$  based on the difference between the center pixel and its neighbors.

3. **Adding Edge Preservation with Diffusivity:** To preserve edges, we adjust the diffusion coefficient dynamically based on the image gradient (sharp changes in pixel values). High gradients indicate edges, so we decrease the diffusivity there to avoid blurring:

- **Compute Gradients:** For pixel (i, j), compute a basic approximation of the gradient magnitude:

$$\text{Gradient} = \sqrt{(u(i+1, j) - u(i-1, j))^2 + (u(i, j+1) - u(i, j-1))^2}$$

- **Calculate Diffusivity:** Based on the gradient, define diffusivity  $g(\text{gradient})$  as:

$$g(\text{gradient}) = \exp\left(-\frac{\text{gradient}^2}{2\sigma^2}\right)$$

This function decreases as the gradient increases, thus slowing diffusion near edges (high gradient regions) while allowing more diffusion in smooth areas.

4. **Final Update Rule with Edge Preservation:** Incorporating diffusivity, the final update rule for each pixel (i, j) is:

$$u(i, j)^{\text{new}} = u(i, j)^{\text{old}} + \alpha \cdot dt \cdot g(\text{gradient}) \cdot \nabla^2 u(i, j)$$

This rule combines the Laplacian with an edge-sensitive diffusivity factor to preserve important structures while smoothing the image.

### Key Properties of Heat Diffusion:

- **Smoothing Effect:** Diffusion of Intensity: The heat equation models the diffusion of intensity values across the image, like the diffusion of heat in a physical system. This process results in a smoothing effect, reducing high-frequency noise.
- **Preservation of Edges and Noise Reduction:** By incorporating a spatially varying diffusion coefficient, the heat equation can selectively smooth regions of the image. In areas of low gradient (smooth regions), the diffusion coefficient is high, leading to significant smoothing. Conversely, in areas of high gradient (edges), the diffusion coefficient is low, preserving edge details. This adaptive smoothing behavior enables the heat equation to balance noise reduction and edge preservation effectively.
- **Flexibility:** The diffusion coefficient can be adjusted to control the degree of smoothing and edge preservation, allowing for customization to specific image characteristics and diagnostic needs.
- **Feature Enhancement:** The modified heat equation can amplify subtle features, such as small variations in the spine curvature, making them more easily detectable by automated detection algorithms.
- **Computational Efficiency:** Compared to some other advanced image processing techniques, the modified heat equation often requires less computational resources, making it suitable for real-world applications.

## 5.2. Anisotropic Diffusion: A Powerful Pre-processing Technique

Anisotropic diffusion is a non-linear filtering technique that selectively smooths image regions while preserving important edges. This property makes it particularly suitable for pre-processing X-ray images for scoliosis detection. By reducing noise in homogeneous regions, anisotropic diffusion enhances the visibility of subtle features like vertebral boundaries, which are crucial for accurate curvature analysis.

**Mathematically, the Anisotropic Diffusion is expressed as:**

$$\frac{\partial I_t(x,y)}{\partial t} = \nabla \cdot (c(|\nabla I_t|) \nabla I_t) \quad [30]$$

Where:

- $I_t(x, y)$  is the image intensity at position  $(x, y)$  and time  $t$ .
- $\nabla$  is the gradient operator.
- $c(|\nabla I_t|)$  is a diffusion coefficient that depends on the gradient magnitude.

### Implementation Steps:

- **Gradient Calculation:** Gradients along both axes are computed using finite differences:
  - For horizontal gradients:

$$grad_x = u(x + 1, y) - u(x-1, y)$$

- For vertical gradients:

$$grad_y = u(x, y + 1) - u(x, y-1)$$

- **Gradient Magnitude:** The magnitude of these gradients is calculated as:

$$grad\ magnitude = \sqrt{(grad_x)^2 + (grad_y)^2}$$

- **Diffusivity Function:** An edge-sensitive diffusivity function is computed based on the gradient magnitude:

$$c(grad\ magnitude) = e^{-\frac{(grad\ magnitude)^2}{2k^2}}$$

This function determines how much smoothing will occur based on local edge strength; areas with high gradient magnitudes (edges) receive less smoothing compared to smoother regions.

- **Divergence Calculation:** The divergence of the diffusivity-weighted gradients is calculated as follows:

- For horizontal divergence:

$$div_x = c(grad_x) \cdot grad_x$$

- For vertical divergence:

$$div_y = c(grad_y) \cdot grad_y$$

- **Image Update:** The original image is updated using a weighted sum of these divergences:

$$u_{new} = u + \alpha \cdot dt \cdot (\nabla \cdot (div_x + div_y))$$

This update rule continues over multiple time steps until the image achieves a desirable level of smoothness with retained structural details.

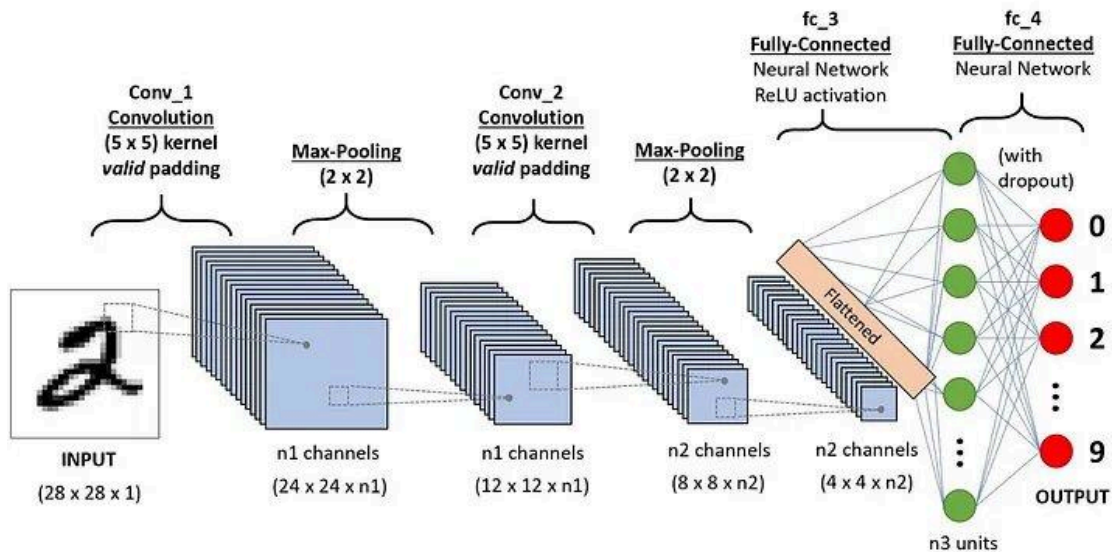
### Key Properties of Anisotropic Diffusion:

- **Edge Preservation:** The diffusion coefficient's behavior near edges results in a phenomenon known as backward diffusion. This effectively enhances edges rather than blurring them.
- **Noise Reduction:** In regions with low gradients (e.g., homogeneous areas), the diffusion coefficient allows for forward diffusion, which helps to smooth out noise.
- **Convergence Speed:** The convergence speed of the diffusion coefficient plays a crucial role in determining the level of edge preservation. A higher convergence speed generally leads to better edge preservation.

Anisotropic diffusion prepares the X-ray images through this controlled diffusion process, creating an optimal balance between clarity and structural detail, essential for subsequent scoliosis detection methods.

### 5.3. Classification Stage using CNN

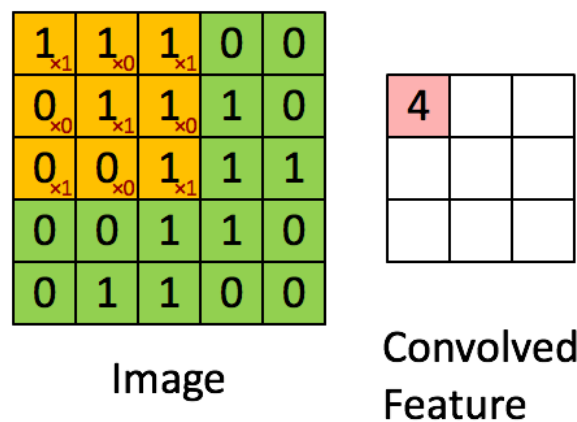
Convolutional Neural Networks (CNNs) are a class of deep learning models specifically designed to process grid-like data, such as images and time series. They have been pivotal in achieving breakthroughs in tasks involving visual data, such as image recognition and computer vision, by efficiently learning spatial hierarchies of features. CNNs are composed of layers like convolutional, pooling, and fully connected layers, which allow them to automatically capture patterns such as edges, textures, and shapes in the input data. This makes them particularly effective for tasks like image classification and object detection. [\[49\]](#)



### 5.3.1. Model Architecture

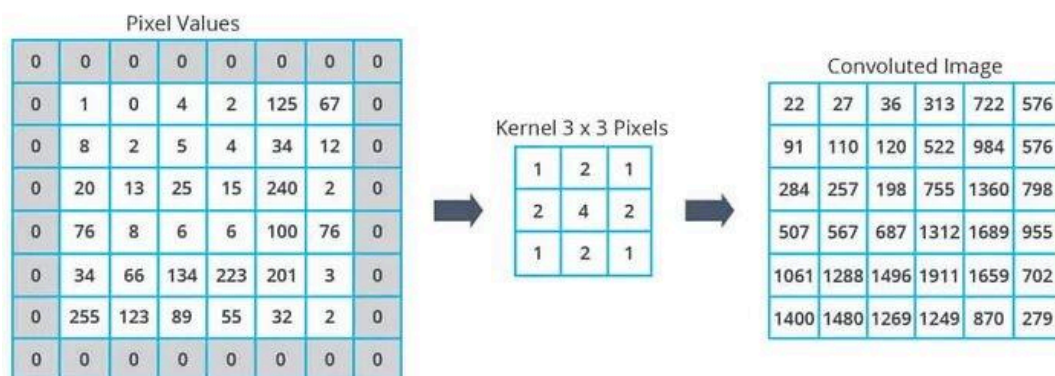
#### i. Convolutional Layer

The convolutional layer is the core building block of a CNN. It performs a mathematical operation called convolution, which involves sliding a filter (or kernel) across the input image and computing dot products between the filter and local regions of the image. This process helps the network learn local patterns, such as edges, corners, and textures. Filters, which are small matrices like 3x3 or 5x5, are trained to detect specific patterns, and multiple filters are often used in each layer to capture diverse features. Parameters like stride (the step size of the filter) and padding (adding extra pixels around the image to preserve spatial dimensions) further refine the operation.



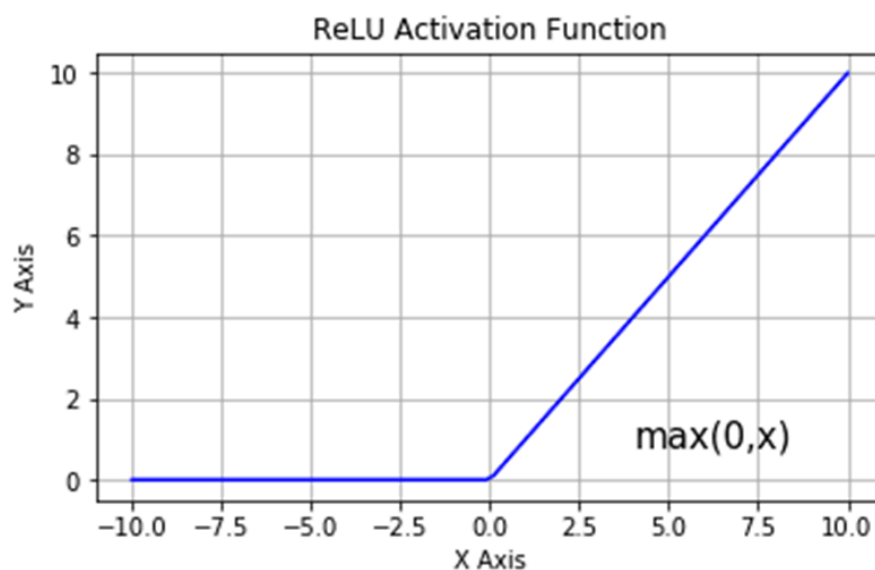
#### ii. Kernel

A kernel, also known as a filter, is a small matrix that plays a crucial role in the convolution operation. This matrix slides across the input data, such as an image, and performs a dot product with the local region of the input to extract features. Kernels are typically small, such as 3x3 or 5x5, and are designed to detect specific patterns like edges, corners, or textures. Each kernel in a CNN learns to recognize a unique pattern, with multiple kernels in a layer capturing diverse features from the input data. The kernel's ability to focus on local regions and share weights across the entire input makes the network efficient and effective in extracting meaningful patterns.



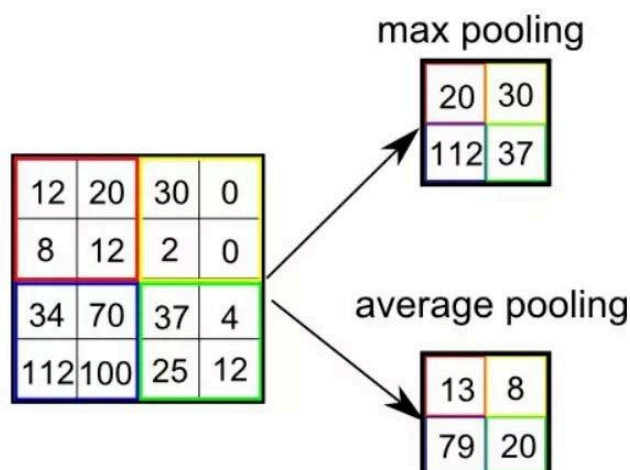
### iii. Activation Function (ReLU)

To introduce non-linearity into the model, an activation function is applied after the convolution operation. A commonly used activation function in CNNs is the Rectified Linear Unit (ReLU), which replaces all negative values in the feature map with zero. This simple operation allows the network to learn complex patterns by enabling it to model non-linear relationships within the data.



### iv. Pooling Layer (Max Pooling)

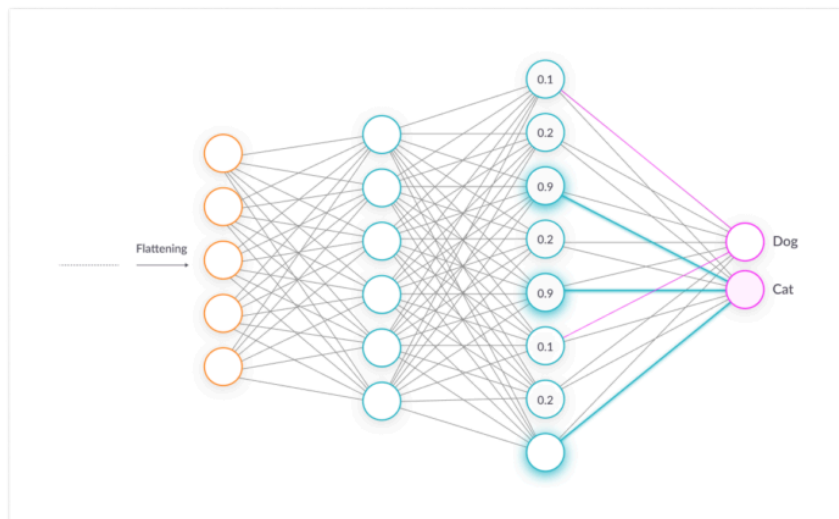
Pooling layers serve to downsample feature maps, reducing their spatial dimensions while retaining the most important information. Max pooling, a widely used operation, selects the maximum value from each local region of the feature map. This not only reduces computational complexity but also makes the network more robust to variations like small translations of objects in the input image. The reduced size of the feature maps also helps mitigate overfitting.





## v. Fully Connected (Dense) Layer

Following the convolutional and pooling layers, the feature maps are flattened into a one-dimensional vector and passed into fully connected layers. These layers, composed of neurons connected to every node in the previous layer, perform the classification task by combining the learned features. The final layer typically employs a softmax or sigmoid activation function to generate class probabilities, producing the model's output. For instance, in a medical imaging scenario, this could be classifying an image as "Normal" or "Scoliosis."

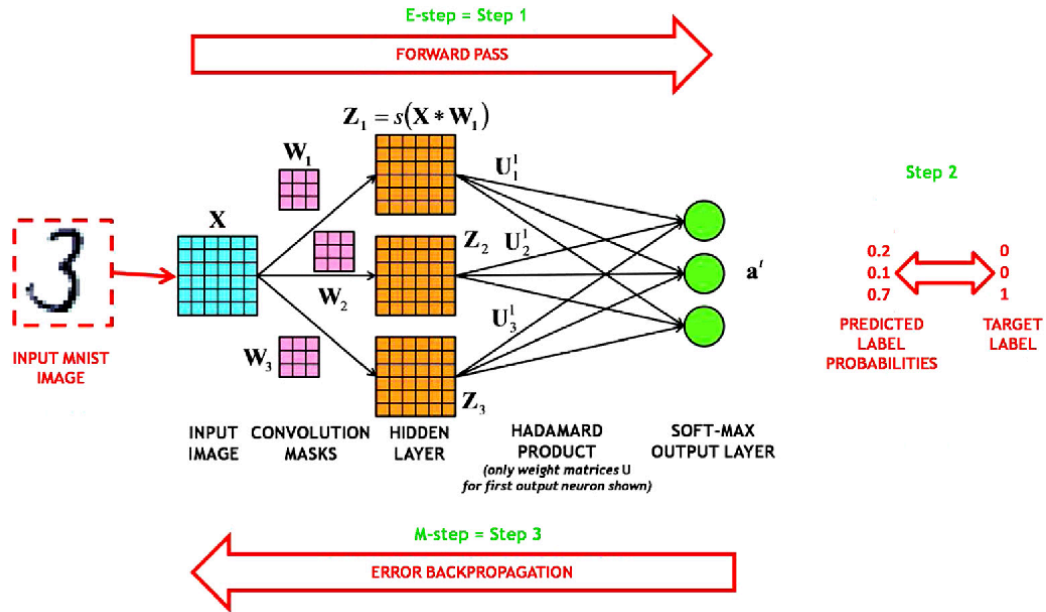


## vi. Forward Propagation in CNNs

The forward propagation process begins with feeding the input (e.g., a grayscale image with dimensions 25x50 pixels) into the CNN. Convolutional layers apply filters to detect low-level features like edges, followed by an activation function like ReLU to introduce non-linearity. Pooling layers then downsample the feature maps, retaining critical information and improving computational efficiency. The feature maps are flattened and passed through fully connected layers for classification, with the final layer providing probabilities for each class.

## vii. Backward Propagation and Model Training

Backward propagation, or backpropagation, is the process used to train the CNN. It starts with calculating the loss between the predicted output and the true label using a loss function, such as categorical cross-entropy. The gradients of the loss function with respect to the model's weights are computed using the chain rule of calculus. These gradients are used to adjust the weights via optimization algorithms like Stochastic Gradient Descent (SGD) or Adam. This process is repeated over multiple iterations (epochs), gradually improving the model's accuracy by minimizing the loss.



## 6. Experimental Work

### 6.1. Introduction to Experimental Setup

This study focuses on developing a Convolutional Neural Network (CNN) model to classify spinal X-ray images as either "Normal" or "Scoliosis." Additionally, the study implements a method for calculating the Cobb angle, a key metric for scoliosis diagnosis, using image processing and edge detection techniques. The workflow integrates preprocessing, training, validation, and post-classification angle measurement to provide an end-to-end solution for scoliosis assessment.

### 6.2. Data Description

#### i. Dataset Overview

The dataset comprises grayscale spinal X-ray images categorized as "Normal" and "Scoliosis," resized to  $25 \times 50$  pixels for standardization. It includes over 580 normal and 580 scoliosis scans, sourced from Egyptian clinics and open datasets. Clinics such as **ARC for Scoliosis Physiotherapy** (Dr. Mahmoud Ibrahim, PhD, PT), **ScolioCare** (Dr. Sarah M. Ali, MSc, PT), **الفقري العمود لتأهيل قوام** (Dr. Tayseer Saber Abdeldayem), and **4Kids Therapy Clinic** (Dr. Sarah M. Ali, MSc, PT) contributed real-world data. Open datasets like the **Mendeley Dataset** ([Link](#)) and **Roboflow Universe** ([Link](#)) provided diverse samples. This mix supports the development of a robust, generalizable scoliosis detection model. The dataset was divided into training and validation subsets, with 10% of the data reserved for validation.

## ii. Data Preprocessing

- Grayscale Conversion: Ensures uniformity as the images originally contained varying color formats.
- Resizing: Standardized to 25×50 pixels.
- Normalization: Pixel values were scaled to the range [0, 1] to stabilize training.

## 6.3. Model Architecture

### i. Input Layer

- **Input Shape:** 25×50×1(gray-scale image).
- **Purpose:** Accepts preprocessed grayscale images and feeds them into the network.

### ii. First Convolutional Layer

- **Layer Type:** Conv2D
- **Number of Filters:** 50
- **Kernel Size:** 3×3
- **Activation Function:** ReLU (Rectified Linear Unit).
- **Features Learned:** Detects low-level features like edges and corners.
- **Input Shape:** 125×50×1
- **Output Shape:** 23×48×50

### iii. First Pooling Layer

- **Layer Type:** MaxPooling2D
- **Pool Size:** 2×2
- **Purpose:** Reduces spatial dimensions by selecting the maximum value in each 2×2 region.
- **Output Shape:** 11×24×50

### iv. Second Convolutional Layer

- **Layer Type:** Conv2D
- **Number of Filters:** 100
- **Kernel Size:** 3×3
- **Activation Function:** ReLU.
- **Features Learned:** Captures more complex patterns and textures.
- **Output Shape:** 9×22×100

### v. Second Pooling Layer

- **Layer Type:** MaxPooling2D
- **Pool Size:** 2×2
- **Purpose:** Further reduces spatial dimensions while retaining critical features.
- **Output Shape:** 4×11×100

#### vi. Third Convolutional Layer

- **Layer Type:** Conv2D
- **Number of Filters:** 100
- **Kernel Size:** 3×3
- **Activation Function:** ReLU.
- **Features Learned:** Extracts high-level abstract features.
- **Output Shape:** 2×9×100

#### vii. First Dense Layer

- **Layer Type:** Flatten
- **Purpose:** Converts the 3D tensor into a 1D vector for input into dense layers.
- **Output Shape:** 1800

#### viii. First Dense Layer

- **Layer Type:** Dense
- **Number of Neurons:** 100
- **Activation Function:** ReLU.

#### ix. Output Layer

- **Layer Type:** Dense
- **Number of Neurons:** 2
- **Activation Function:** Softmax.
- **Purpose:** Outputs probabilities for the two classes ("Normal" and "Scoliosis").
- **Purpose:** Learns high-level combinations of extracted features.

## 6.4. Training Methodology

### i. Dataset Splitting

The dataset was divided into:

- **Training Set:** 90% of the data.
- **Validation Set:** 10% of the data.

### ii. Hyperparameters

- **Batch Size:** 50.
- **Number of Epochs :** 20.
- **Optimizer:** Adam.
- **Loss Function:** Sparse Categorical Crossentropy
- **Evaluation Metric:** Accuracy

The model was trained using TensorFlow's `model.fit()` method, which tracked both training and validation performance.

## 6.5. Image Preprocessing for Cobb Angle Calculation

To calculate the Cobb angle, a combination of edge detection and advanced filtering techniques was applied:

### i. Edge Detection

- **Algorithm:** Canny edge detection.
- **Parameters:** Thresholds of 50 and 150.
- **Purpose:** Identifies the boundaries of vertebrae in spinal X-rays.

### ii. Line Detection

- **Algorithm:** Hough Line Transform.
- **Parameters:** Minimum line length = 50, Maximum line gap = 15.
- **Purpose:** Detects lines corresponding to vertebral boundaries.

### iii. Angle Clustering

- **Algorithm:** K-means clustering.
- **Number of Clusters:** 2
- **Purpose:** Groups detected angles into two clusters for Cobb angle computation.

### iv. Heat Equation Simulation

$$\text{Equation: } \frac{\partial y}{\partial t} = \alpha \nabla^2 u$$

- $\alpha = 0.03$  (Thermal diffusivity).
- $\Delta t = 0.1$  (Time Step).
- Number of Steps: 25.

**Purpose:** Smoothens the image while preserving edges, improving line detection

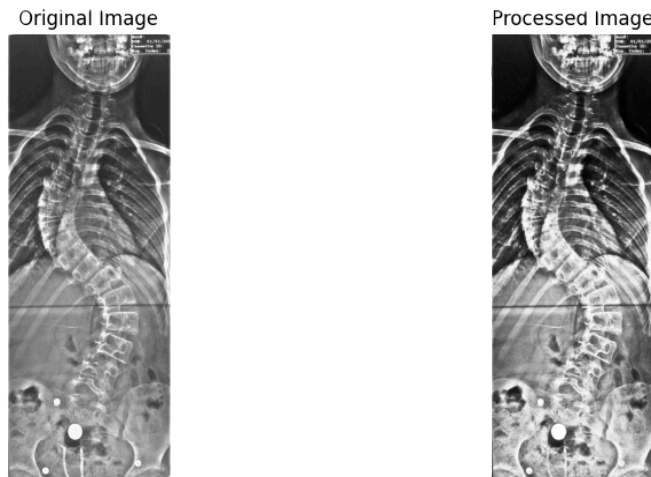
## 7. Results

### 7.1. Comparison of Heat Equation and Anisotropic Diffusion for Pre-processing Spinal X-ray Images

In this study, we evaluated the effectiveness of the heat equation and anisotropic diffusion for pre-processing spinal X-ray images. Both methods were applied to a dataset of noisy X-ray images, and their performance was assessed in terms of noise reduction, edge preservation, and overall image quality.

#### Heat Equation

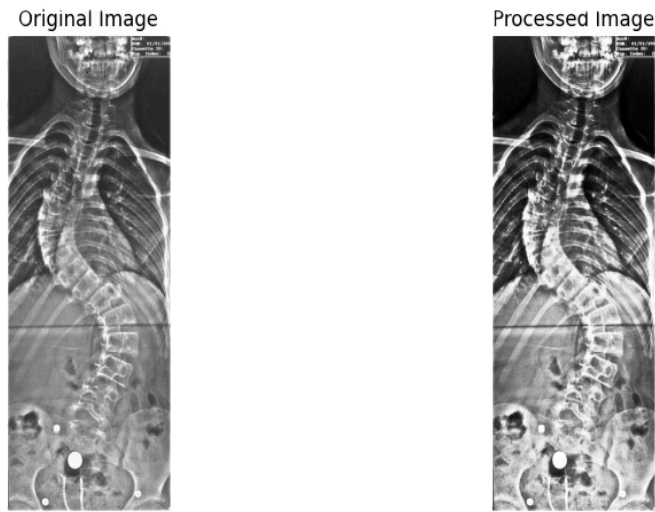
- **Noise Reduction:** The heat equation effectively reduced noise in the images, particularly in regions with low-frequency noise. However, it also tended to blur edges, especially in regions with high-frequency noise.
- **Edge Preservation:** The heat equation's isotropic diffusion nature limited its ability to preserve sharp edges. While it could reduce noise, it often compromised the fine details of the spinal structures.



*Heat Equation Pre-processing Result*

#### Anisotropic Diffusion

- **Edge Preservation:** Anisotropic diffusion demonstrated superior edge preservation capabilities. By adaptively adjusting the diffusion coefficient based on the image gradient, it effectively prevented the blurring of edges, especially in regions with high-frequency noise.
- **Noise Reduction:** While it was effective in reducing noise, particularly in homogeneous regions, anisotropic diffusion may not be as effective as the heat equation in reducing low-frequency noise.












*Anisotropic Diffusion Pre-processing Result*

## Experimental results and discussion

In this study, we evaluated the effectiveness of the heat equation and anisotropic diffusion for pre-processing spinal X-ray images. Both methods were applied to a dataset of noisy X-ray images, and their performance was assessed in terms of noise reduction, edge preservation, and overall image quality.

### Overall Comparison

<i>Noisy Image</i>	<i>Heat Equation</i>	<i>Anisotropic Diffusion</i>
		
		
		

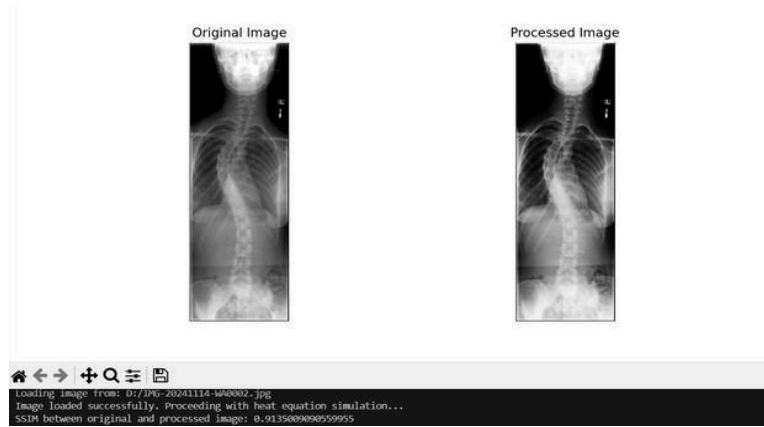
## 7.2. Structural Similarity Index Measurements (SSIM)

$$SSIM(I_o, I_r) = \frac{(2\mu_x\mu_y + \alpha)(2cov(I_o, I_r) + \beta)}{(\mu_x^2 + \mu_y^2 + \alpha)(\sigma_x^2 + \sigma_y^2 + \beta)} \quad [47]$$

where  $\mu_x$  and  $\mu_y$  are the means and  $\sigma_x$  and  $\sigma_y$  are the variances of the images  $I_o$  and  $I_r$  respectively.  $cov(I_o, I_r)$  is the covariance of the two images, and  $\alpha, \beta$  are small values, used to stabilize the division with small denominators. SSIM is used to show the similarity of the structure of the input image to the structure of the restored image. The SSIM lies between 0 and 1. The higher value of SSIM shows a great structural similarity between the input and restored image.

### SSIM Result for Heat Equation

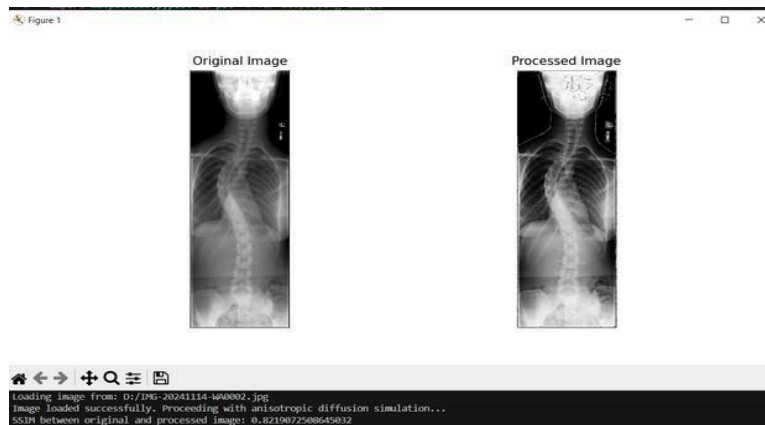
The heat equation resulted in a Structural Similarity Index Measurements (SSIM) score of 0.9135, indicating good perceptual quality.



*SSIM Result for Heat Equation*

### SSIM Result for Anisotropic Diffusion:

The anisotropic diffusion resulted in a Structural Similarity Index (SSIM) score of 0.8219, indicating a lower level of perceptual similarity.



*SSIM Result for Anisotropic Diffusion*



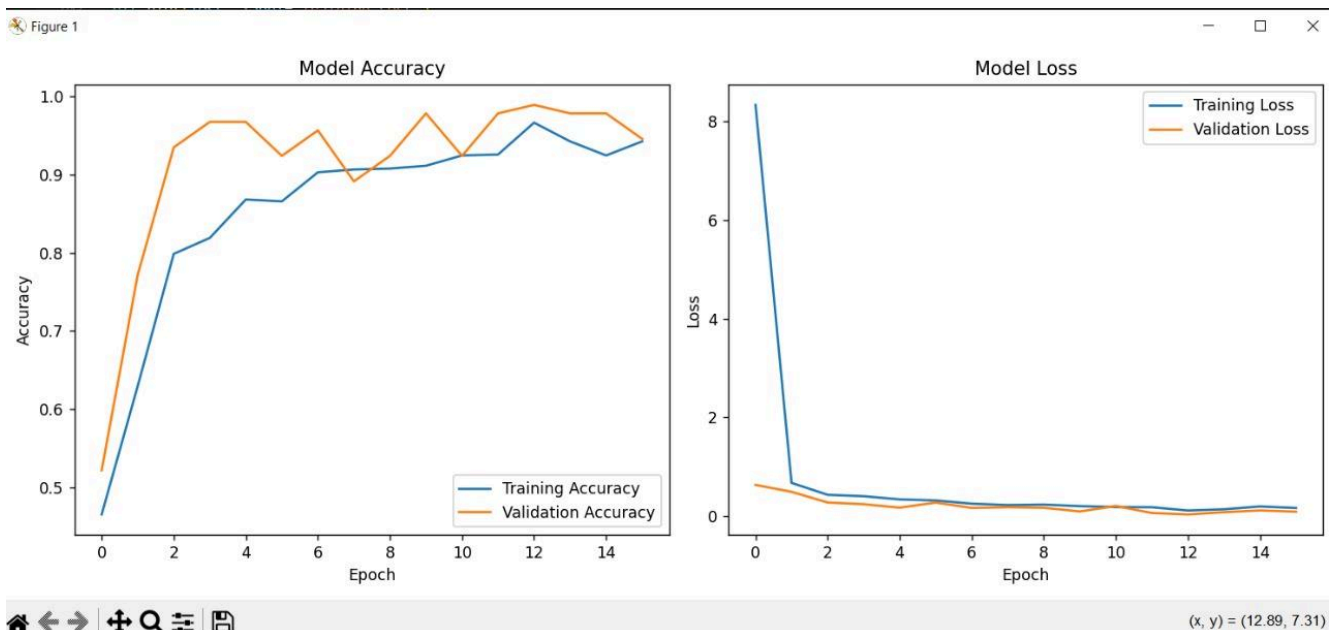
### 7.3. Results of the CNN model's performance

The training results demonstrate steady improvement in accuracy and loss over 20 epochs. The training accuracy increases from 0.8657 to a peak of 0.9664, while the training loss decreases from 0.3207 to 0.1168 before stabilizing. Validation accuracy remains consistently high, peaking at 0.9891, with validation loss dropping significantly from 0.2780 to 0.0371. These results indicate strong model generalization and performance, with no clear signs of overfitting by the final epoch.

```
17/17 - 1s - 42ms/step - accuracy: 0.8657 - loss: 0.3207 - val_accuracy: 0.9239 - val_loss: 0.2780
Epoch 7/20
17/17 - 1s - 42ms/step - accuracy: 0.9029 - loss: 0.2552 - val_accuracy: 0.9565 - val_loss: 0.1708
Epoch 8/20
17/17 - 1s - 42ms/step - accuracy: 0.9065 - loss: 0.2280 - val_accuracy: 0.8913 - val_loss: 0.1847
Epoch 9/20
17/17 - 1s - 44ms/step - accuracy: 0.9077 - loss: 0.2374 - val_accuracy: 0.9239 - val_loss: 0.1731
Epoch 10/20
17/17 - 1s - 44ms/step - accuracy: 0.9113 - loss: 0.2059 - val_accuracy: 0.9783 - val_loss: 0.0976
Epoch 11/20
17/17 - 1s - 45ms/step - accuracy: 0.9245 - loss: 0.1870 - val_accuracy: 0.9239 - val_loss: 0.2094
Epoch 12/20
17/17 - 1s - 43ms/step - accuracy: 0.9257 - loss: 0.1838 - val_accuracy: 0.9783 - val_loss: 0.0666
Epoch 13/20
17/17 - 1s - 48ms/step - accuracy: 0.9664 - loss: 0.1168 - val_accuracy: 0.9891 - val_loss: 0.0371
Epoch 14/20
17/17 - 1s - 48ms/step - accuracy: 0.9424 - loss: 0.1417 - val_accuracy: 0.9783 - val_loss: 0.0831
Epoch 15/20
17/17 - 1s - 46ms/step - accuracy: 0.9245 - loss: 0.1999 - val_accuracy: 0.9783 - val_loss: 0.1186
Epoch 16/20
17/17 - 1s - 42ms/step - accuracy: 0.9424 - loss: 0.1682 - val_accuracy: 0.9457 - val_loss: 0.0932
```

*CNN's Model Accuracy*

Training and validation performance of the CNN model for normal and scoliosis classification. The left panel shows the accuracy metrics, where the model achieves high accuracy on both training and validation datasets, indicating strong learning capability. The right panel depicts the loss metrics, where both training and validation losses decrease and converge over epochs, demonstrating effective training stability.



*Summary statistics of the CNN model's performance on the test dataset.*

## 7.4. Training and Validation Metrics of the CNN Model for Scoliosis Classification

Summary statistics of the CNN model's performance on the test dataset. Out of 240 images, the model correctly predicted 203 cases, resulting in a test accuracy of 84.58%. The model incorrectly classified 37 images, with a test loss of 0.7369, indicating a moderate level of error. These results highlight the model's effectiveness in classifying normal and scoliosis images, though there is still room for improvement.

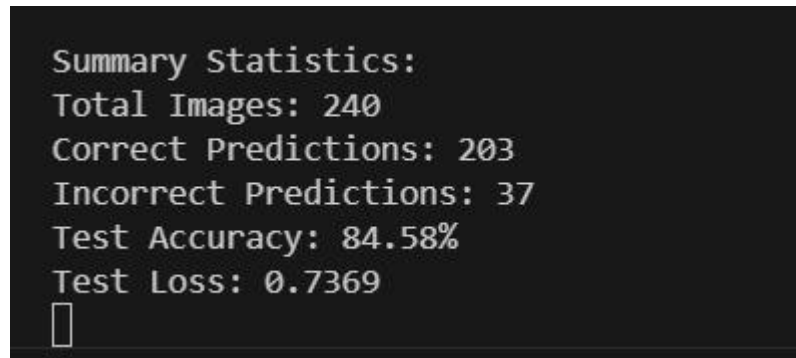


*Figure of Training and validation performance of the CNN model for normal and scoliosis classification.*

The bar chart illustrates the performance of the trained model on the testing dataset. The green bar represents the number of correct predictions made by the model, while the red bar represents incorrect predictions. Out of a total of 240 images in the test dataset, the model accurately classified 203 images, corresponding to a correct prediction rate of approximately 84.58%. The remaining 37 images were misclassified, accounting for about 15.42% of the total. This visualization highlights the model's effectiveness in differentiating between the "Normal" and "Scoliosis (Scol)" classes in the test set.

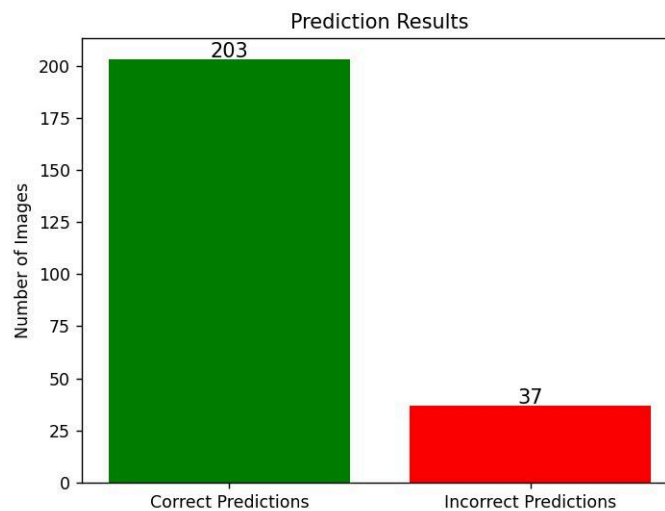


*Figure of bar chart showing the testing dataset*

## 8. Conclusion

In this study, we compared the performance of the heat equation and anisotropic diffusion for pre-processing spinal X-ray images. While anisotropic diffusion is often considered a superior technique for preserving edges and reducing noise, our results suggest that the heat equation may be more suitable for certain types of images, particularly those with lower levels of noise and less pronounced edge features. The heat equation achieved a higher SSIM score, indicating better perceptual quality. However, for images with significant noise and complex structures, anisotropic diffusion may still be the preferred choice. Further research is needed to optimize the parameters of both techniques and to develop more advanced pre-processing methods that can better preserve the delicate details of spinal structures while effectively reducing noise.

## 9. References

1. Tajdari, M., Pawar, A., Li, H., Tajdari, F., Maqsood, A., Cleary, E., Saha, S., Zhang, Y. J., Sarwark, J. F., and Liu, W. K. (2021). Image-based modeling for Adolescent Idiopathic Scoliosis: Mechanistic machine learning analysis and prediction. *Computer Methods in Applied Mechanics and Engineering*, 374, 113590. <https://doi.org/10.1016/j.cma.2020.113590>
2. Zalevsky, Z., Livshits, P., & Gur, E. (2014). New approaches to image processing based failure analysis of nano-scale ULSI devices. Elsevier. <https://doi.org/10.1016/C2013-0-06953-8>
3. Göreke, V. (2022). A novel method based on Wiener filter for denoising Poisson noise from medical X-ray images. *Biomedical Signal Processing and Control*, 79, 104031. <https://doi.org/10.1016/j.bspc.2022.104031>
4. Mohd Sagheer, S. V., and George, S. N. (2020). A review on medical image denoising algorithms. *Biomedical Signal Processing and Control*, 61, 102036. <https://doi.org/10.1016/j.bspc.2020.102036>
5. Rundo, L., Tangherloni, A., Nobile, M. S., Militello, C., Besozzi, D., Mauri, G., and Cazzaniga, P. (2019). MedGA: A novel evolutionary method for image enhancement in medical imaging systems. *Expert Systems With Applications*, 119, 387-399. <https://doi.org/10.1016/j.eswa.2018.11.013>
6. Kleinstreuer, C., Childress, E., and Kennedy, A. (2013). Targeted drug delivery: Multifunctional nanoparticles and direct micro-drug delivery to tumors. In S. M. Becker & A. V. Kuznetsov (Eds.), *Transport in biological media* (pp. 391–416). Elsevier. <https://doi.org/10.1016/B978-0-12-415824-5.00010-2>
7. Kong, W., Miao, Q., Liu, R., Lei, Y., Cui, J., and Xie, Q. (2022). Multimodal medical image fusion using gradient domain guided filter random walk and side window filtering in the framelet domain. *Information Sciences*, 585, 418-440. <https://doi.org/10.1016/j.ins.2021.11.033>
8. Ou, X., Chen, X. Xu, X., Xie, L. Chen, X., Hong, Z., Bai, H., Liu, X., Chen, Q., Li, L. (2021). Recent Development in X-Ray Imaging Technology: Future and Challenges. *Research*. DOI: [10.34133/2021/9892152](https://doi.org/10.34133/2021/9892152)
9. Takahide, O., Shigeru, F., Hiroshi, I., Shin'ya, Y., Jianming, L., Yahagi, T. (2004). Noise Reduction in Digital Radiography Using Wavelet Packet Based on Noise Characteristics. *Journal of Signal Processing*. 8. 485-494. 10.2299/jsp.8.485.
10. Nowak, R. D. and Richard B. (1999). "Wavelet-domain filtering for photon imaging systems." *IEEE transactions on image processing: a publication of the IEEE Signal Processing Society* 8 5: 666-78.
11. Wang, L., Lu, J., Li, Y., Yahagi, T., and Okamoto, T. (2005). Noise Reduction Using Wavelet with Application to Medical X-ray Image. *IEEE International Conference on Industrial Technology*. doi: [10.1109/icit.2005.1600606](https://doi.org/10.1109/icit.2005.1600606)
12. Yang, X.S., and Papa, J. P. (2016). Bio-inspired computation and applications in image processing. Elsevier Ltd. <https://doi.org/10.1016/C2015-0-00856-5>
13. Claude, K., and Zwicker, M., (2014). "Progressive image denoising." *IEEE transactions on image processing* 23, no. 7: 3114-3125
14. Priyam, Ch., and Milanfar, P., (2009). "Is denoising dead?" *IEEE Transactions on Image Processing* 19(4): 895-911.
15. Kaur, H., Virmani, J., & Thakur, S. (2018). A genetic algorithm-based metaheuristic approach to customize a computer-aided classification system for enhanced screen film mammograms. *U- Healthcare Monitoring Systems*, 217-259. <https://doi.org/10.1016/B978-0-12-815370-3.00010-4>
16. Mafi, M., Martin, H., Cabrerizo, M., Andrian, J., Barreto, A., & Adjouadi, M. (2019). A comprehensive survey on impulse and Gaussian denoising filters for digital images. *Signal Processing*, 157, 236-260. <https://doi.org/10.1016/j.sigpro.2018.12.006>

17. Gupta, B., and Lamba, S. S. (2021). An efficient anisotropic diffusion model for image denoising with edge preservation. *Computers & Mathematics With Applications*, 93, 106-119. <https://doi.org/10.1016/j.camwa.2021.03.029>
18. Nakamura, S., Kobayashi, T., Funatsu, A. (2016). Patient radiation dose reduction using an X-ray imaging noise reduction technology for cardiac angiography and intervention. *Heart Vessels* 31, 655– 663 <https://doi.org/10.1007/s00380-015-0667-z>
19. ten Cate, T., van Wely, M., Gehlmann, H. (2015). Novel X-ray image noise reduction technology reduces patient radiation dose while maintaining image quality in coronary angiography. *Neth Heart J* 23, 525–530 <https://doi.org/10.1007/s12471-015-0742-1>
20. Rapp, B. E. (2017). *Microfluidics: Modeling, mechanics and mathematics*. Elsevier Inc. <https://doi.org/10.1016/C2012-0-02230-2>
21. Bovik, A. L. (2005). *Handbook of image and video processing*. Elsevier Inc. <https://doi.org/10.1016/B978-0-12-119792-6.X5062-1>
22. Frangi, A. F., Prince, J. L., and Sonka, M. (2024). *Medical image analysis*. Elsevier Ltd. <https://doi.org/10.1016/C2015-0-06316-X>
23. Wang, S., Celebi, M. E., Zhang, Y., Yu, X., Lu, S., Yao, X., Zhou, Q., Miguel, M., Tian, Y., Gorriz, J. M., & Tyukin, I. (2021). Advances in Data Preprocessing for Biomedical Data Fusion: An Overview of the Methods, Challenges, and Prospects. *Information Fusion*, 76, 376-421. <https://doi.org/10.1016/j.inffus.2021.07.001>
24. Guy, G., Sochen, N., and Zeevi, Y. Y. (2002) Forward-and-backward diffusion processes for adaptive image enhancement and denoising. *IEEE transactions on image processing* 11, (7): 689-703.
25. Pietro, P., and Malik, J. (1990) Scale-space and edge detection using anisotropic diffusion. *IEEE Transactions on pattern analysis and machine intelligence* 12, (7): 629-639.
26. Dost, R., & Kasiviswanathan, K. (2022). Analyses of drought severity and frequency in Afghanistan. *Developments in Environmental Science*, 14, 259-275. <https://doi.org/10.1016/B978-0-443-18640-0.00014-6>
27. Yuan, X., Nayoze-Coynel, C., Shaigan, N., Fisher, D., Zhao, N., Zamel, N., Gazdzicki, P., Ulsh, M., Friedrich, K. A., Girard, F., & Groos, U. (2021). A review of functions, attributes, properties and measurements for the quality control of proton exchange membrane fuel cell components. *Journal of Power Sources*, 491, 229540. <https://doi.org/10.1016/j.jpowsour.2021.229540>
28. Dimian, A. C., Bildea, C. S., & Kiss, A. A. (2013). Chemical Product Design. *Computer Aided Chemical Engineering*, 35, 489-523. <https://doi.org/10.1016/B978-0-444-62700-1.00012-7>
29. Adamo, F., Attivissimo, F., Di Nisio, A., & Savino, M. (2009). A low-cost inspection system for online defects assessment in satin glass. *Measurement*, 42(9), 1304-1311. <https://doi.org/10.1016/j.measurement.2009.05.006>
30. Gupta, B., and Lamba, S. S. (2021). An efficient anisotropic diffusion model for image denoising with edge preservation. *Computers & Mathematics With Applications*, 93, 106-119. <https://doi.org/10.1016/j.camwa.2021.03.029>
31. Bouget, D., Allan, M., Stoyanov, D., & Jannin, P. (2016). Vision-based and marker-less surgical tool detection and tracking: A review of the literature. *Medical Image Analysis*, 35, 633-654. <https://doi.org/10.1016/j.media.2016.09.003>
32. Arora, J. S. (2003). More on Numerical Methods for Unconstrained Optimum Design. *Introduction to Optimum Design (Second Edition)*, 305-337. <https://doi.org/10.1016/B978-012064155-0/50009-4>
33. Ziyang, Z., Duan, Ch., Lin, T., Zhou, Sh., Wang, Y. and Gao, X. (2020).GVFOM: a novel external force for active contour-based image segmentation. *Information Sciences* 506: 1-18.

34. ,W., Ren, W.,and Wang,H., (2013).Anisotropic second and fourth order diffusion models based on convolutional virtual electric field for image denoising." Computers & Mathematics with Applications 66(10):1729-1742.
35. Ovidiu, G., and Whelan, P.F. (2010). A new GVF-based image enhancement formulation for use in the presence of mixed noise." Pattern Recognition 43(8): 2646-2658.
36. Zhang, Q., Yang, L. T., Chen, Z., & Li, P. (2018). A survey on deep learning for big data. Information Fusion, 42, 146-157. <https://doi.org/10.1016/j.inffus.2017.10.006>
37. Yuan-Quan,W., Guo,J., Chen,W. and Zhang,W. (2013). Image denoising using modified Perona– Malik model based on directional Laplacian. Signal Processing 93(9): 2548-2558.
38. Mannan, S. (2013). Computer Aids and Expert Systems. Lees' Process Safety Essentials, 383-401. <https://doi.org/10.1016/B978-1-85617-776-4.00020-8>
39. Baraha, S., Sahoo, A. K., & Modalavalasa, S. (2022). A systematic review on recent developments in nonlocal and variational methods for SAR image despeckling. Signal Processing, 196, 108521. <https://doi.org/10.1016/j.sigpro.2022.108521>
40. Cristovao,C., Foi, A., Katkovnik,V. and Egiazarian,K. (2018).Nonlocality-reinforced convolutional neural networks for image denoising." IEEE Signal Processing Letters 25( 8) :1216-1220.
41. Saeed,A. and Barnes,N.( 2019).Real image denoising with feature attention. In Proceedings of the IEEE/CVF international conference on computer vision, 3155-3164.
42. Chunwei, T., Xu,Y., and Zuo,W. (2020).Image denoising using deep CNN with batch renormalization. Neural Networks 121: 461-473.
43. Prabhu, G.K. (2012). Automatic Quantification of Spinal Curvature in Scoliotic Radiograph using Image Processing. J Med Syst 36, 1943–1951. <https://doi.org/10.1007/s10916-011-9654-9>
44. Dubost, F. (2020). Automated estimation of the spinal curvature via spine centerline extraction with ensembles of cascaded neural networks. In Y. Cai, L. Wang, M. Audette, G. Zheng, and S. Li (Eds.), Computational methods and clinical applications for spine imaging. CSI 2019. Lecture notes in computer science (Vol. 11963). Springer, Cham. [https://doi.org/10.1007/978-3-030-39752-4\\_10](https://doi.org/10.1007/978-3-030-39752-4_10)
45. Tajdari, M., Pawar, A., Li, H., Tajdari, F., Maqsood, A., Cleary, E., Saha, S., Zhang, Y. J., Sarwark, J. F., & Liu, W. K. (2021). Image-based modelling for Adolescent Idiopathic Scoliosis: Mechanistic machine learning analysis and prediction. Computer Methods in Applied Mechanics and Engineering, 374, 113590. <https://doi.org/10.1016/j.cma.2020.113590>
46. Claudio,V., Wafa,S., and Laurent,G. (2020). A convolutional neural network to detect scoliosis treatment in radiographs. International Journal of Computer Assisted Radiology and Surgery. 15. 10.1007/s11548-020-02173-4.
47. Bakurov, I., Buzzelli, M., Schettini, R., Castelli, M., & Vanneschi, L. (2022). Structural similarity index (SSIM) revisited: A data-driven approach. Expert Systems With Applications, 189, 116087. <https://doi.org/10.1016/j.eswa.2021.116087>
48. Frangi, A. F., Prince, J. L., & Sonka, M. (2024). Medical Image Analysis. Elsevier Ltd. <https://doi.org/10.1016/C2015-0-06316-X>
49. U. Kose, D. Gupta, D. A. V. H. C., and A. Khanna, “Chapter 7 - Deep convolutional neural network–based image classification for COVID-19 diagnosis,” in Data Science for covid-19, Amsterdam: Academic Press, 2021.

**Link to our Repository on Github:**

<https://github.com/RaghadAbdelhameed/ARC.git>